

We are IntechOpen, the world's leading publisher of Open Access books Built by scientists, for scientists

6,900

Open access books available

186,000

International authors and editors

200M

Downloads

Our authors are among the

154

Countries delivered to

TOP 1%

most cited scientists

12.2%

Contributors from top 500 universities



WEB OF SCIENCE™

Selection of our books indexed in the Book Citation Index
in Web of Science™ Core Collection (BKCI)

Interested in publishing with us?
Contact book.department@intechopen.com

Numbers displayed above are based on latest data collected.
For more information visit www.intechopen.com



Chromia Evaporation in Advanced Ultra-Supercritical Steam Boilers and Turbines

Gordon R. Holcomb

*National Energy Technology Laboratory, United States Department of Energy, Albany, OR
USA*

1. Introduction

Goals of the U.S. Department of Energy's Advanced Power Systems Initiatives include power generation from coal at 60% efficiency, which requires steam conditions of up to 760 °C and 340 atm, so-called advanced ultra-supercritical (A-USC) steam conditions. Similar efforts are underway in Europe, Japan, and China to raise efficiencies by raising steam temperatures to 700 °C and above. A limitation to achieving the goal is a lack of cost-effective metallic materials that can perform at these temperatures and pressures. Some of the more important performance limitations are high-temperature creep strength, fireside corrosion resistance, and steam-side oxidation resistance. Nickel-base superalloys are expected to be the materials best suited for steam boiler and turbine applications above about 675 °C (Viswanathan et al., 2005). Specific alloys of interest include Haynes 230 and 282, Inconel 617, 625, and 740, Nimonic 263. Alloy compositions are given in Table 1 (Haynes International, 2008a, 2008b; Special Metals Corporation, 2004a, 2004b, 2005, 2006). Steam-side oxidation can result in several adverse effects: general section loss from material thinning, deep localized section loss from internal oxidation (that may also provide crack initiation sites), reduced heat transfer due to the development of insulating oxide layers (that may lead to higher metal temperatures to maintain the same steam conditions), dimensional changes that are critical in airfoils, and downstream erosion from oxide spallation. Evaporation of protective chromia scales may also be an issue at the higher temperatures and pressures of A-USC steam turbines. The evaporation of chromia scales in steam is the focus of the research presented here.

Water vapor is known to adversely affect the oxidation behavior of chromia-forming alloys. Several explanations have been developed to explain the observed behaviors (Essuman et al., 2008; Young & Pint, 2006). Some are briefly described:

- Increased chromia growth rates from the doping of Cr₂O₃ with hydrogen species that result from the oxidation reaction between the metal and H₂O (Norby, 1993; Hänsel et al., 2003 as cited in Young & Pint, 2006). Similar increased growth rates were found for the oxidation of Cr containing dissolved hydrogen compared to Cr without dissolved hydrogen (Henry et al., 2001 as cited in Essuman et al., 2008).
- Enhanced growth stresses that lead to scale cracking (Schütze et al., 2004 as cited in Essuman et al., 2008).
- Enhanced internal oxidation of Cr by water vapor changing the solubility or diffusivity of oxygen in the alloy (Essuman et al., 2008). Increases in internal oxidation can also

lead to scales with less Cr_2O_3 formation and thus increased tendencies to breakaway oxidation (Essuman et al., 2008).

- Rapid, or “breakaway” oxidation from the depletion of Cr in the scale resulting from reactive evaporation of Cr_2O_3 in the presence of O_2 and H_2O (Essuman et al., 2008; Holcomb, 2008, 2009; Young & Pint, 2006). Clear links to evaporation were shown by how increased gas flow rates led to faster breakaway oxidation and increased Fe:Cr ratios within the oxide scale (Asteman et al., 2000).

Alloy	Fe	Cr	Ni	Co	Mo	Ti	Al	Mn	Other	C_{Cr}°
Haynes 230	1.5	22	Bal	2.5	2		0.3	0.5	0.02 La 14 W 0.4 Si 0.1 C 75 B	38000
Haynes 282	0.75	19.5	Bal	10	8.5	2.1	1.5		0.15 Cu 0.075 Si 0.06 C 50 B	31000
Inconel 617	1.5	22	Bal	12.5	9	0.3	1.15	0.5	0.25 Cu 0.5 Si 0.1 C 30 B	35400
Inconel 625	2.5	21.5	Bal	0.5	9	0.2	0.2	0.25	3.65 Nb 0.25 Si 0.05 C	34900
Inconel 740	0.7	25	Bal	20	0.5	1.8	0.9	0.3	2 Nb 0.5 Si 0.03 C	38700
Nimonic 263	0.35	20	Bal	20	5.85	2.15	0.3	0.3	0.1 Cu 0.2 Si 0.06 C 25 B	32200

Table 1. Nominal alloy compositions (wt%, except for B which is in ppm) and bulk alloy Cr concentrations (C_{Cr}° , mol/m³) for alloys of interest (Haynes International, 2008a, 2008b; Special Metals Corporation, 2004a, 2004b, 2005, 2006). Source values that were ranges are listed as the midpoint of the range. Source values that were maximums are listed as half the maximum. For economic reasons it is not unusual for actual chemical compositions of materials delivered for use in power plants to be near the lower end of the specification. Only Nb is listed for sources that gave a value or range for Nb+Ta. Source values for Pb, P, S and Bi are omitted.

This last behavior based on reactive evaporation of Cr_2O_3 is the subject of the work presented here. In prior work, a methodology to calculate the expected chromia evaporation rate as a function of temperature, pressure, gas velocity, and steam chemistry was developed for chromia forming alloys (Holcomb, 2008). The methodology was experimentally validated at low pressures and gas velocities by how well its kinetics

predictions matched atmospheric pressure oxidation experiments in air plus water vapor environments. At 760 °C and 340 atm, evaporation rates as high as 5.18×10^{-8} kg/m²/s of CrO₂(OH)₂(g) were predicted for rotating high pressure (HP) turbine blade components (Holcomb, 2008). This is equivalent to 0.08 mm per year of solid Cr loss. It was speculated that chromia evaporation upstream of the HP turbine, such as in the superheater, could partially saturate the steam with CrO₂(OH)₂(g) and reduce the chromia evaporation rate.

The above efforts were expanded (Holcomb, 2009) to include 1) the use of new determinations of the thermodynamic properties of CrO₂(OH)₂(g) (Opila et al., 2007), 2) expanding the methodology from flat plate components to cylindrical geometries (such as found within superheaters and steam pipes), 3) linking the chromia evaporation in steam to Cr diffusion within the alloy to predict alloy Cr concentration profiles and breakaway oxidation times, and 4) applying the breakaway oxidation predictions to a hypothetical superheater-steam pipe-HP turbine steam path, where the effects of CrO₂(OH)₂(g) saturation along the steam path are applied. In many aspects this was similar to the work of Young and Pint (2006).

Presented here is further validation of the model by examining the reactive evaporation effects resulting from exposure of Haynes 230 and Haynes 282 to moist air environments as a function of flow rate and water content. These two alloys differ in Ti and Mn contents, which may form outer layers of TiO₂ or Cr-Mn spinels, which would in theory decrease the evaporation of Cr₂O₃ from the scale (Holcomb & Alman, 2006).

2. Chromia evaporation

The oxidation of alloys protected by the formation of Cr₂O₃ (chromia formers) can undergo scale loss due to reactive evaporation of chromium-containing gas species. Water vapor increases the evaporation loss by allowing the formation of CrO₂(OH)₂(g), which for these conditions has a higher vapor pressure than CrO₃(g). CrO₃(g) is the predominate Cr gas specie in dry air or oxygen (Graham & Davis, 1971). The formation of CrO₂(OH)₂(g) can be written as:



The equilibrium partial pressure of CrO₂(OH)₂(g) can be found from Eq. 2, where ΔG_1° is the Gibbs energy of reaction 1, R is the gas constant, T is the absolute temperature, K₁ is the equilibrium constant of reaction 1, $a_{\text{Cr}_2\text{O}_3}$ is the activity of Cr₂O₃, and P_i is the partial pressure of gas specie i.

$$\Delta G_1^\circ = -RT \ln K_1 = -RT \ln \frac{P_{\text{Cr}_2(\text{OH})_2}}{a_{\text{Cr}_2\text{O}_3}^{1/2} P_{\text{H}_2\text{O}} P_{\text{O}_2}^{3/4}} \quad (2)$$

Even while maintaining a Cr₂O₃ scale, evaporation can change the overall oxidation kinetics from parabolic behavior to linear kinetics or even to breakaway oxidation. Linear kinetics can arise after scale growth from oxidation, which decreases with increasing scale thickness, matches the scale loss from reactive evaporation (Tedman, 1966). The change in scale thickness, x, with time, t, can then be described in terms of the parabolic rate constant, k_p, and the linear reactive evaporation rate, k_e, as:

$$\frac{dx}{dt} = \frac{k_p}{x} - k_e \quad (3)$$

At long times or high reactive evaporation rates, a limiting scale thickness, x_L , arises that is given by:

$$x_L = \frac{k_p}{k_e} \quad (4)$$

In this case metal loss rates are linear, but still involve diffusion through a protective scale. Rapid metal loss can occur when reactive evaporation of Cr depletes the scale (and sometimes the substrate metal) of Cr (Asteman et al., 1999, 2000). Decreased Cr in the scale or metal can lead to the formation of less protective oxides, such as Fe-Cr oxides in Fe-Cr base alloys. Unprotective scales can lead to rapid metal loss, or “breakaway” oxidation.

A detailed methodology for calculating evaporation rates in a variety of environments was presented in earlier work for gas flow over a flat plate (Holcomb, 2008). Two basic equations were developed: Eq. 5 for laminar flow and Eq. 6 for turbulent flow:

$$k_e \left(\frac{\text{kg}}{\text{m}^2\text{s}} \right) = 0.664 Re_L^{0.5} Sc^{0.343} \frac{D_{AB} M_{\text{CrO}_2(\text{OH})_2}}{LRT} P_{\text{CrO}_2(\text{OH})_2} \quad (5)$$

$$k_e \left(\frac{\text{kg}}{\text{m}^2\text{s}} \right) = 0.0592 Re_L^{0.8} Sc^{0.333} \frac{D_{AB} M_{\text{CrO}_2(\text{OH})_2}}{LRT} P_{\text{CrO}_2(\text{OH})_2} \quad (6)$$

where Re_L and Sc are the dimensionless Reynolds and Schmidt numbers, D_{AB} is the gaseous diffusion coefficient between $\text{CrO}_2(\text{OH})_2$ and the solvent gas (m^2/s), $M_{\text{CrO}_2(\text{OH})_2}$ is the molecular mass of $\text{CrO}_2(\text{OH})_2$ ($\text{kg}/\text{g-mol}$), L is the length (m) in the flow direction of the flat plate, $P_{\text{CrO}_2(\text{OH})_2}$ is the partial pressure of $\text{CrO}_2(\text{OH})_2$ (atm), R is the gas constant ($8.20594 \times 10^{-5} \text{ m}^3\text{atm}/\text{K g-mol}$), and T is the absolute temperature (K). The dimensionless Reynolds and Schmidt numbers are defined as:

$$Re_L = \frac{\rho_s u L}{\eta} \quad (7)$$

$$Sc = \frac{\eta}{\rho_s D_{AB}} \quad (8)$$

where ρ_s is the density of the solvent gas (kg/m^3), η is the absolute viscosity ($\text{kg}/\text{m}/\text{s}$), and u is the gas velocity (m/s). Values for two key parameters in Eqs. 5-8 (D_{AB} and η) are not established and require estimates (Holcomb, 2008) to be made.

The diffusion coefficient, D_{AB} , was estimated with a method using a $T^{1.75}/P_T$ relationship and “diffusion volumes” (Fuller et al., 1966; Holcomb, 2008), where P_T is total pressure. This estimate was later improved (Holcomb, 2009) using a computed geometry for $\text{Cr}_2(\text{OH})_2(\text{g})$ (Opila et al., 2007) to estimate the “diffusion volumes”. The diffusion coefficient estimate in supercritical steam was further adjusted (reduced) based on methods presented by Bird et al. (1960) and Slattery and Bird (1958).

The absolute viscosity, η , was estimated for gas mixtures using the semi empirical formulation of Wilke (Wilke, 1950 as cited in Gaskell, 1992) that combines the absolute

viscosity of the component gases. For non-polar gases, η was estimated based on the Lennard_jones potential (Gaskell, 1992). For water and steam, information of η as a function of T and P was used (Stultz & Kitto, 1992).

The Gibbs energy for reaction 1, (Opila et al., 2007), was used to determine $P_{CrO_2(OH)_2}$. This is a change from the prior work (Holcomb, 2008), where the thermodynamic data of Gindorf et al. (2001) was used. The differences in Gibbs energies for reaction 1 between the two transpiration studies (Gindorf et al., 2001, Opila et al., 2007) are shown in Table 2. The Opila values result in higher $P_{CrO_2(OH)_2}$ values (Eq. 2) and was attributed to possible undercounting of Cr loss in the Gindorf study and to the wider range in water vapor contents that allowed more precision in measurements at higher water levels (Opila et al., 2007).

Source	ΔH_x° , J mol ⁻¹	ΔS_x° , J mol ⁻¹	Notes
Opila et al., 2007	53500 ± 5400	-45.6 ± 6.6	Based on second law enthalpy and entropy methods from transpiration experiments to determine $\Delta H_{861}^\circ = 53.5$ kJ mol ⁻¹ and $\Delta S_{861}^\circ = 45.6$ J mol ⁻¹ K ⁻¹ at the average temperature of 861 K.
Gindorf et al., 2001	61400	-49.8	Based on transpiration experiments to determine $\ln P_{Cr_2(OH)_2}$ (Pa) to be equal to $0.442 + -7387.5T^{-1}$ with an average temperature of 948 K in air with 2% H ₂ O.

Table 2. Simplified ΔG_T° formulations based on the approximation that ΔG_T° varies linearly with temperature for most substances (Kubaschewki & Alcock, 1979), where $\Delta G_T^\circ = \Delta H_x^\circ - T\Delta S_x^\circ$ and x is an elevated temperature close to the desired T.

The above methodology for flat surfaces (Eqs. 5-6) was expanded for use in pipes and to include possible saturation effects (Holcomb, 2009). Equations 5-6 were written in more general terms that included the average Sherwood number (Sh_{Ave}) and that allowed for the value of the partial pressure of $CrO_2(OH)_2(g)$ well away from the metal surface, $P_{CrO_2(OH)_2}^\circ$, to slow down the evaporation (Eqs. 4-5 assumed $P_{CrO_2(OH)_2}^\circ$ was zero), Eq. 9. Here Sh_{Ave} is equal to $0.664Re_L^{0.5}Sc^{0.343}$ for laminar flow over flat plates and to $0.0592Re_L^{0.8}Sc^{0.333}$ for turbulent flow over flat plates.

$$k_e \left(\frac{kg}{m^2s} \right) = Sh_{Ave} \frac{D_{AB}M_{CrO_2(OH)_2}}{LRT} \left(P_{CrO_2(OH)_2} - P_{CrO_2(OH)_2}^\circ \right) \quad (9)$$

For flow within circular tubes, Eq. 9 was used but with a different expression for Sh_{Ave} . For the analysis that follows, the Dittus-Boelter equation (Winterton, 1998; Incropera & DeWitt, 2001) was used for Sh_{Ave} for turbulent conditions:

$$Sh_{Ave} = 0.023Re_d^{0.8}Sc^{0.4} \quad (10)$$

where Re_d is the same as Re_L but with the diameter, d, instead of the plate length, L, in Eq. 7. For rough pipes the use of an expression for Sh_{Ave} that incorporates a friction factor, such as that of Petukov (Incropera & DeWitt, 2001; Petukhov, 1970) can be used.

One additional point is that the evaporation rate, k_e , from Eq. 9 is for the amount of $Cr_2(OH)_2(g)$ leaving the surface, while the mass change data will be in terms of $Cr_2O_3(s)$ lost

from the surface. The conversion is shown in Eq. 11 (Holcomb, 2008). Unless otherwise stated, k_e is on a $\text{Cr}_2(\text{OH})_2(\text{g})$ basis.

$$k_{e, \text{Cr}_2\text{O}_3} = \frac{M_{\text{Cr}_2\text{O}_3}}{2M_{\text{CrO}_2(\text{OH})_2}} k_{e, \text{CrO}_2(\text{OH})_2} = 0.644 k_{e, \text{CrO}_2(\text{OH})_2} \quad (11)$$

3. Chromia evaporation in cyclic oxidation tests

Cyclic oxidation tests were conducted for up to 2000 hourly cycles in moist air. Each hourly cycle consisted of 55 minutes in the furnace, withdrawal from the furnace, holding for 3.4 minutes, and then placement back into the furnace. The remaining 1.6 minutes per hourly cycle was the travel time the samples took into and out of the furnace. The samples experienced rapid heating and cooling rates, and were oriented such that the gas flow was parallel to their surfaces. More experimental details can be found in prior work (Holcomb et al., 2007).

A goal of the cyclic tests was to evaluate alloys for use in A-USC boilers and turbines. Scale exfoliation, resulting in part from thermal expansion mismatch between the alloy and the scale, is an important failure mechanism in boiler tubes (Wright & Tortorelli, 2007). The use of thermal cycles is an aggressive test of scale exfoliation tendencies. While some alloys did exhibit scale exfoliation in the cyclic tests (Holcomb et al., 2007), except as noted no scale exfoliation was observed during tests on the alloys discussed below.

Results for two alloys from prior work (Holcomb, 2008, 2009), Haynes 230 and Inconel 740, are shown in Figs. 1 and 2 respectively, and also in Table 3. The Haynes 230 results show the influence of gas velocity—a factor of 4 increase in gas velocity resulted in a factor of 2 increase in evaporation, which is consistent with Eqs. 7 and 9. The dashed lines in Fig. 1 show the evaporation rate from the model, with an activity of chromia of 0.05. This low chromia activity presumably arises from chromia depletion in the outer portion of the oxide scale as chromia is lost to evaporation. The results for two different heats of Inconel 740 in Fig. 2 show two different behaviors. The heat with the \square symbols initially had a similar evaporation rate as the Haynes 230 results. The evaporation rate decreased after about 800 cycles. The other heat, with + symbols, exhibited much less chromia evaporation. One difference between the two heats was 1.6 Ti in the heat with the \square symbols compared with 1.8 Ti in the heat with + symbols.

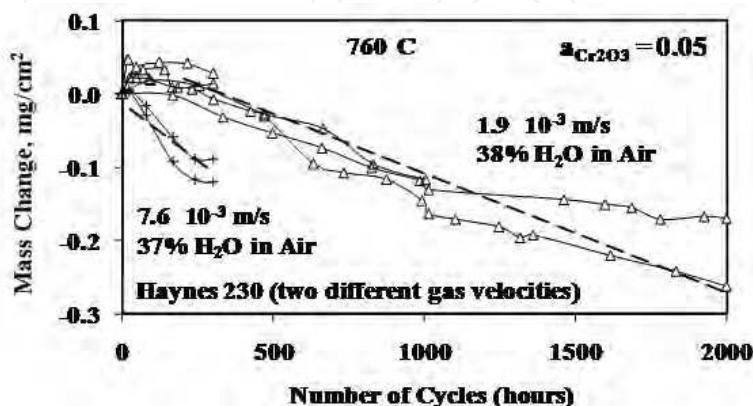


Fig. 1. Mass change measurements for Haynes 230 exposed at 760 °C in moist air at two different gas velocities. The dotted lines are the predicted mass change due to chromia evaporation with a chromia activity of 0.05. Adapted from Holcomb (2009).

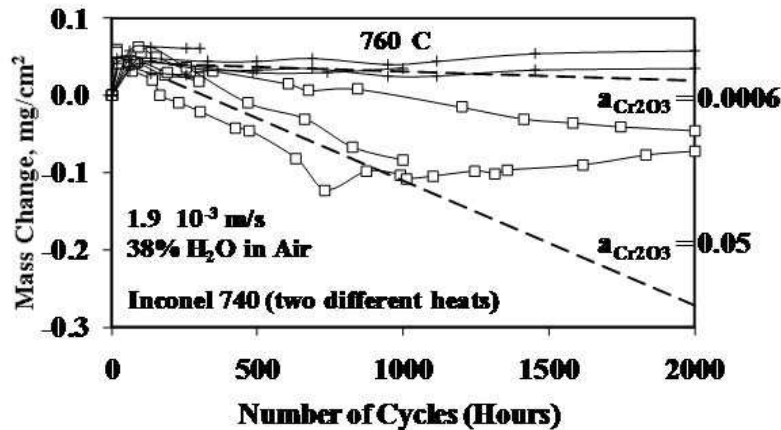


Fig. 2. Mass change measurements for two different heats of Inconel 740 exposed at 760 °C in moist air. The dotted lines are the predicted mass changes due to chromia evaporation with chromia activities of 0.05 and 0.0006. Adapted from Holcomb (2009).

Results for Haynes 230 and Haynes 282 at 800 °C are shown in Figs. 3-4 for two water vapor levels and two gas flow rates, and are also shown in Table 3. The results for Haynes 230 continue to show the same gas velocity dependence shown at 760 °C—a four-fold increase in flow rate doubles the evaporation rate. For Haynes 282, the combination of the highest flow rate and water vapor percentage changed behavior after 1000-12000 cycles. Past this point, small amounts of debris were found upon handling the sample for weighing. So the mass loss was a combination of chromia evaporation and scale spallation. A four-fold increase in flow rate increased, but did not double evaporation rate for Haynes 282. It could well be the case that steady state evaporation was not yet reached for the Haynes 282 prior to it starting to spall.

When the results in Figs. 3-4 were compared with the chromia evaporation model, chromia activities were found that matched the results—found in the last column in Table 3. One thought from prior research (Holcomb, 2009) was that chromia activities would decrease with higher rates of evaporation. As chromia leaves the surface, Mn and Ti oxides would become enriched and thus decrease the chromia activity. Table 3 shows that this is not always the case. Increasing the flow rate while maintaining a constant $P_{\text{H}_2\text{O}}$ resulted in chromia activities of Haynes 230 and Haynes 282 dropping from 0.14 to 0.11 and 0.21 to 0.07, respectively. However, raising the $P_{\text{H}_2\text{O}}$ from 0.19 to 0.57 while maintaining a constant flow rate increased the evaporation rate but also increased the chromia activity for Haynes 230 (0.06 to 0.11). The expected result was found for Haynes 282 with a decrease from 0.12 to 0.07.

Scanning electron microscopy (SEM) was used to examine the surfaces of the 800 °C samples, Fig. 5. The surface structure of Haynes 230 was finer than that found on Haynes 282. The Haynes 282 at the fastest chromia evaporation rate (lower right-hand image in Fig. 5) shows holes in the structure. One could speculate that these holes were where chromia may have evolved from and thus undercut the outer oxide. This undercutting appears to have resulted in the scale spalling in this sample.

The use of x-ray diffraction (XRD) on these surfaces showed chromia and spinels on Haynes 203 and chromia, spinels, and TiO_2 on Haynes 282. Various Cr-Ni-Mn containing spinels have very similar XRD peaks, making identification of Mn-containing spinels impossible.

Alloy	T, °C	P _{H₂O}	Flow Rate, m/s	k _e [Cr ₂ O ₃], kg/m ² s	Time Range, hr	Apparent a _{Cr₂O₃}
Haynes 230	760	0.37	1.9×10 ⁻³	3.8×10 ⁻¹⁰	200-2000	~0.05
Haynes 230	760	0.37	7.6×10 ⁻³	11.7×10 ⁻¹⁰	94-2000	~0.05
Inconel 740	760	0.38	1.9×10 ⁻³	1.5×10 ⁻¹⁰ 5.5×10 ⁻¹⁰	102-2000 18-734	~0.0006 ~0.05
Haynes 230	800	0.19	4.2×10 ⁻³	3.4×10 ⁻¹⁰	200-2000	0.06
Haynes 230	800	0.57	1.0×10 ⁻³	4.9×10 ⁻¹⁰	24-2000	0.14
Haynes 230	800	0.57	4.2×10 ⁻³	9.1×10 ⁻¹⁰	24-2000	0.11
Haynes 282	800	0.19	4.2×10 ⁻³	4.9×10 ⁻¹⁰	600-2000	0.12
Haynes 282	800	0.57	1.0×10 ⁻³	6.1×10 ⁻¹⁰	500-2000	0.21
Haynes 282	800	0.57	4.2×10 ⁻³	7.2×10 ⁻¹⁰	125-1000	0.07

Table 3. Alloys, conditions, and results for cyclic oxidation tests. Gas flow rates are at temperature. Data for 760 °C are from prior work (Holcomb, 2008). Data for Inconel 740 are from the heat with □ points in Fig. 2.

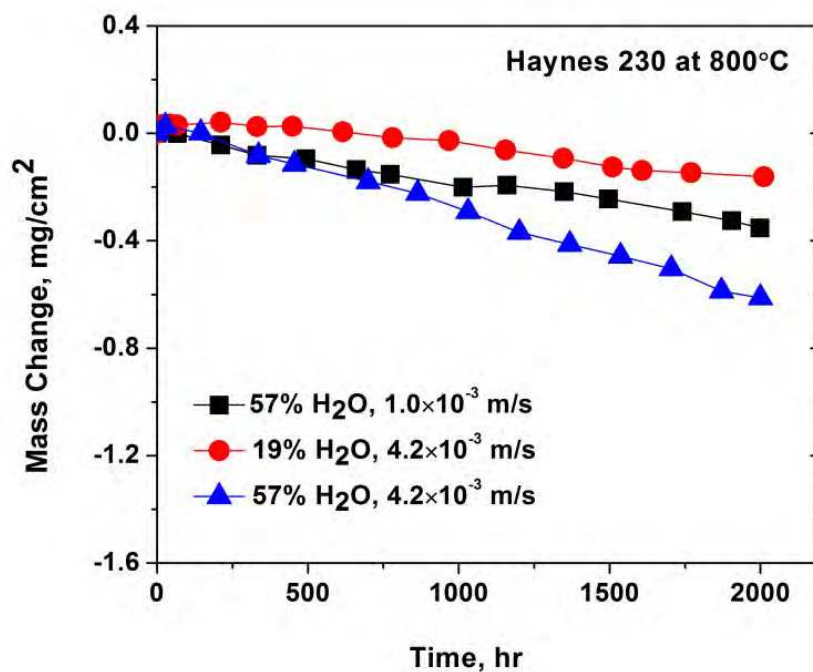


Fig. 3. Mass change measurements Haynes 230 at 800 °C in moist air at three different water vapor levels and gas flow rates.

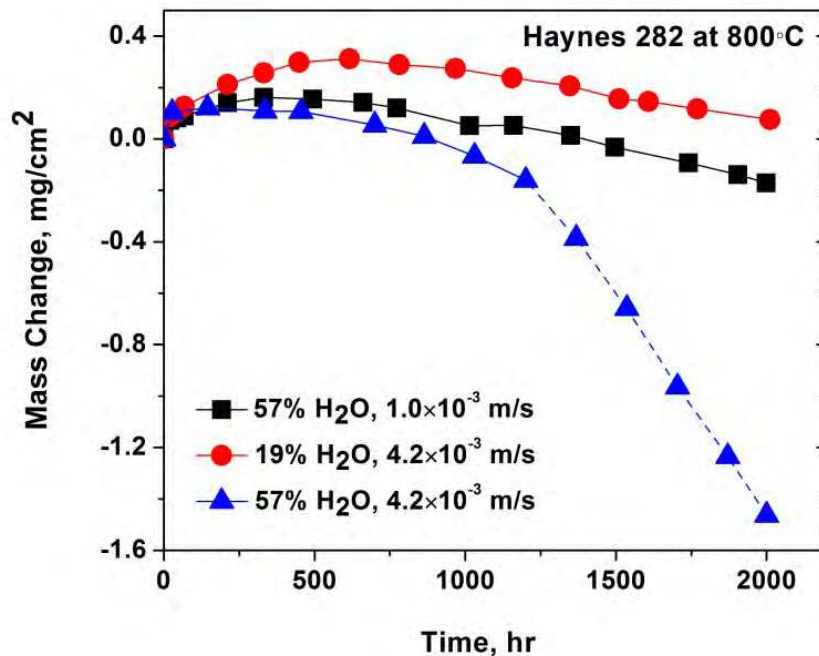


Fig. 4. Mass change measurements Haynes 282 at 800 °C in moist air at three different water vapor levels and gas flow rates. The dashed line indicates spalling.

Elemental spot analyses on the Haynes 230 surface for the slowest chromia evaporation sample (19% H₂O, 4.2×10⁻³ m/s) did not show any Mn on the surface. Analyses of the other two samples, with higher evaporation rates, showed Mn throughout the surface (along with Cr and O).

Elemental spot analyses on all of the Haynes 282 surfaces showed two distinct types of areas within a fine structure. Figure 6 shows a higher magnification image of this surface and these two types of areas. The smaller grains are primarily Cr and O (with smaller amounts of Ni and Al), and the larger grains (with flat surfaces) to be essentially pure Ti and O.

4. Chromium diffusion

After evaporation causes the overall oxidation kinetics to become linear and to have a steady state scale thickness (Eq. 4), the flux of Cr away from the scale via evaporation must equal the flux of Cr to the scale via Cr diffusion within the alloy. If there is insufficient arrival of Cr to the surface, then the chromia scale will not be maintained and breakaway oxidation would be expected to eventually occur.

To model Cr diffusion within the alloy with a constant flux of Cr leaving the surface, the transient heat transfer model of Incropera and DeWitt (Incropera & DeWitt, 2001) within a semi-infinite solid and with a constant surface heat flux was used. The underlying mathematics between heat and mass transfer are the same, so this model was used with appropriate mass transfer parameters. The overall equation for the concentration of Cr as a function of x (depth from the surface into the alloy, m) and t (time, s), $C_{Cr}(x,t)$ is:

$$C_{Cr}(x,t) = C_{Cr}^{\circ} - \frac{2k_e}{M_{CrO_2(OH)_2}} \sqrt{\frac{t}{\pi D_{Cr}}} \exp\left(-\frac{x^2}{4D_{Cr}t}\right) + \frac{k_e x}{M_{CrO_2(OH)_2} D_{Cr}} \operatorname{erfc}\left(\frac{x}{2\sqrt{D_{Cr}t}}\right) \quad (12)$$

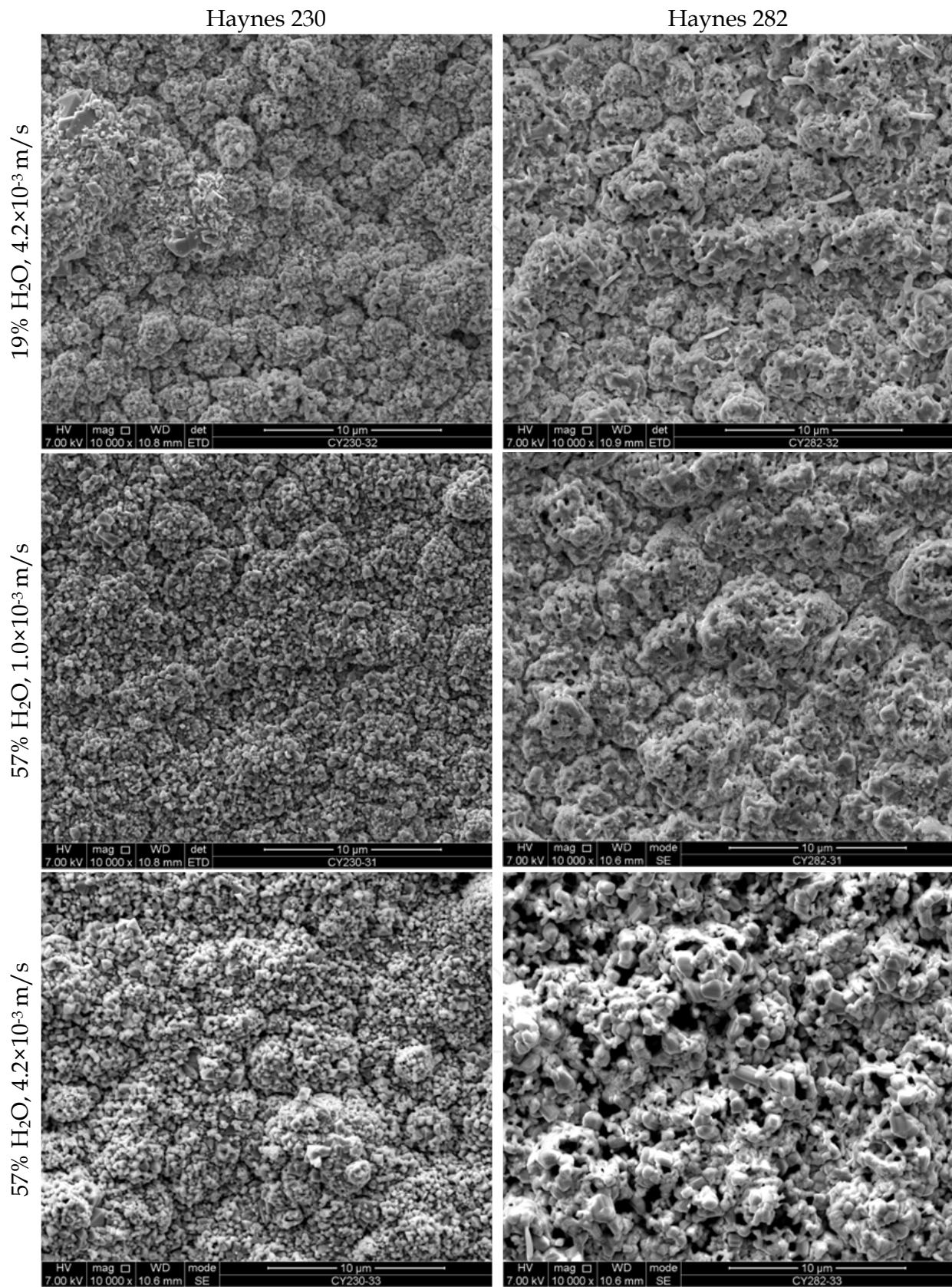


Fig. 5. Surface SEM after 2000 cycles at 800 °C in moist air.

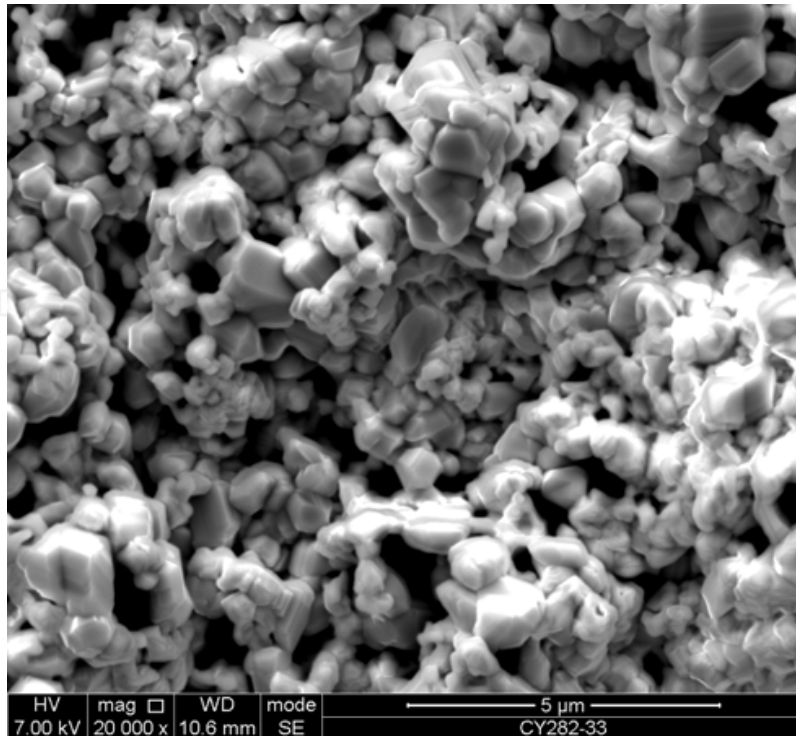


Fig. 6. Secondary electron image of Haynes 282 after 2000 hourly cycles at 800 °C in moist air (57% H₂O) and a gas flow rate of 4.2×10⁻³ m/s. Elemental spot analysis shows the smaller grains to be primarily Cr and O (with smaller amounts of Ni and Al), and the larger grains (with flat surfaces) to be essentially pure Ti and O

where C_{Cr}° is the bulk alloy Cr concentration (mol/m³) (Table 1), D_{Cr} is the diffusion coefficient of Cr (m²/s), and erfc is the complementary error function. For the concentration of Cr at the surface as a function of time, Eq. 12 simplifies to Eq. 13.

$$C_{Cr}(0,t) = C_{Cr}^{\circ} - \frac{2k_e}{M_{CrO_2(OH)_2}} \sqrt{\frac{t}{\pi D_{Cr}}} \quad (13)$$

And the surface concentration is equal to zero at time t^* , as shown in Eq. 14.

$$t^* = \frac{\pi D_{Cr}}{4} \left(\frac{M_{CrO_2(OH)_2} C_{Cr}^{\circ}}{k_e} \right)^2 \quad (14)$$

Breakaway oxidation is expected to occur prior to t^* , such as when the surface concentration becomes less than the critical value required to sustain a Cr₂O₃ scale. The critical value could be estimated, as was done for the critical bulk concentration of Cr in Fe-Cr alloys (Meier et al., 2010), if sufficient diffusion rates in the metal and scale are known. However, the lower bound on the critical value of the surface concentration is zero. So t^* is used as a proxy for the time until breakaway oxidation will occur.

At the temperatures in a steam turbine, the diffusion coefficient, D_{Cr} , is an effective diffusion coefficient and is a combination of lattice, D_{Cr}^L , and grain boundary, D_{Cr}^{gb} , diffusion. The relationship used is based on cubic grains of size λ (m) and with grain boundary width δ (m) (Peng et al., 2005):

$$D_{Cr} \cong D_{Cr}^L + \frac{2\delta}{\lambda} D_{Cr}^{gb} \quad (15)$$

The lattice diffusion coefficients were determined using Dictra diffusion simulation software (Thermo-Calc Software AB, 2006) with the Ni-DATA (Saunders, 2000) and MOB2 (Royal Institute of Technology, 1999) databases. Figure 7 shows lattice diffusion coefficients of Cr in the face-centered-cubic (FCC) phase for several alloys of interest as a function of Cr content at 760 °C. The right-most-point for each alloy is at the alloy Cr content. The lower Cr content values represent the alloy where it is locally depleted in Cr near the surface. Figure 7 shows that for many of the alloys an assumption of a constant value for the diffusion coefficient is a good one.

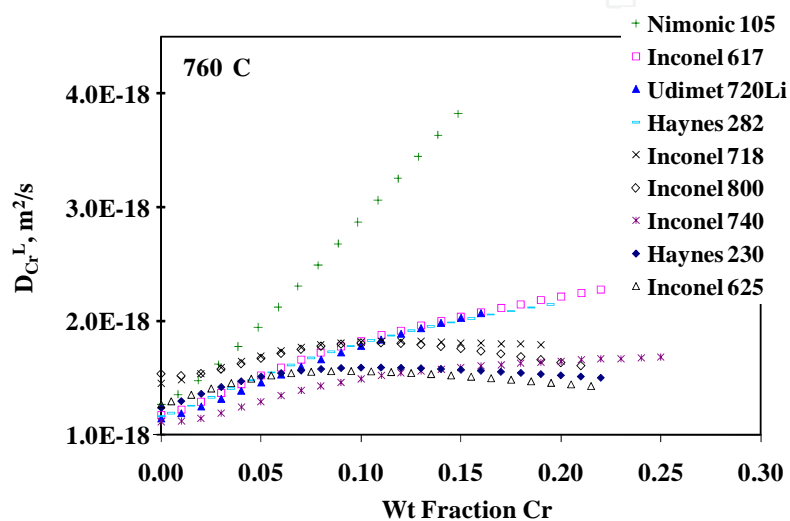


Fig. 7. Lattice diffusion coefficients at 760 °C for Cr in the FCC phase of nickel base superalloys determined using Dictra diffusion simulation software (Thermo-Calc Software AB, 2006) with the Ni-DATA (Saunders, 2000) and MOB2 (Royal Institute of Technology, 1999) databases.

The use of the FCC phase as the basis of lattice diffusion is a simplification of the rather complex nature of these alloys. All of the alloys in Fig. 7 are strengthened by the formation of one or more second phases, the amount of which depends upon heat treatment. Two of these alloys (Nimonic 105 and Udimet 720Li) have very significant amounts of a second phase (gamma prime). The ordered structure of these second phases should result in diffusivities that are much smaller than the FCC phase. So this simplification would tend to overstate the overall effective diffusion coefficients.

Further phase complications can arise from Cr depletion, where the loss of Cr can itself lead to phase changes. An example of this can be seen in Fig. 8, for Inconel 617 exposed to 2000 hourly cycles at 760 °C in air with 37% H₂O at atmospheric pressure (Holcomb, 2009). Figure 8 shows a phase transition zone near the oxide interface, presumably from Cr depletion. Internal oxidation, mainly of aluminum, is also present underneath the oxide scale along grain boundaries. Thus, a more comprehensive phase-based treatment of diffusion coefficients may be warranted. However, for the calculations that follow, the values used for the lattice diffusion coefficients are ones from the FCC phase at the Cr content of the alloy (Fig. 7).

Grain boundary diffusion coefficients are estimated based on the work of Paul *et al.* (Paul *et al.*, 1994) where lattice and grain boundary diffusion coefficients were determined for Inconel 800 (where a grain boundary width of 0.5 nm was used). The estimate is to use the same ratio of grain boundary diffusion to lattice diffusion that was found for Inconel 800, and to use the same grain boundary width of 0.5 nm. This ratio is given by Eq. 16.

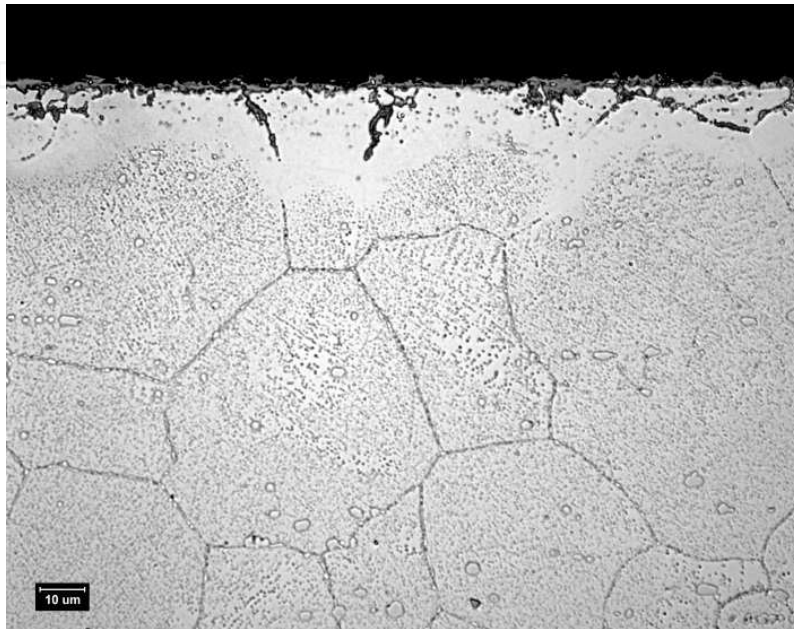


Fig. 8. Results of cyclic oxidation of Inconel 617 at 760 °C in air plus 37% H₂O after 2000 hourly cycles (Holcomb, 2009). A bright field image after etching (50% concentrated nitric acid, 50% glacial acetic acid). A precipitate free zone lies beneath internal oxidation areas.

$$\frac{D_{Cr}^{gb}}{D_{Cr}^L} \cong \exp\left(\frac{12412}{T} - 1.7203\right) \quad (16)$$

An example of a comparison between calculated and measured Cr diffusion profiles is given in Figs. 9-10 for Inconel 740 exposed to 2000 hourly cycles at 760 °C (under the same conditions as in Fig 8). Figure 9 is a backscattered electron image of a cross-section of the metal-scale interface. It shows a very thin oxide scale and a larger thickness of internal oxidation. The internal oxidation is primarily of aluminum and titanium. This kinetic data for this specimen are the points in Fig. 2 with the most mass loss. Figure 10 shows the Cr concentration profile measured using X-ray photoelectron spectroscopy (points) and the results of the model of Eqs. 12 and 16 with λ equal to 50 μm , δ equal to 0.5 nm (line), and k_e of 8.0×10^{-10} kg/m²s. This evaporation rate is the model prediction with an $a_{Cr_2O_3}$ of 0.4. The model is a close fit to the measured points. Note that the use of 2000 hours in Fig. 10 is an approximation that overstates the time at temperature (each hourly cycle had a few minutes at lower temperatures). If the predicted evaporation rate using pure chromium is used ($a_{Cr_2O_3}$ of 1), the predicted evaporation rate is 2.0×10^{-9} kg/m²s, and the model would predict too much Cr loss (a wt fraction of Cr of 0.05 at the surface).

The model curve in Fig 10 invoked an $a_{Cr_2O_3}$ of 0.4. Is lowering the chromia activity valid? These alloys are not pure Ni-Cr alloys and have other alloying elements that oxidize, are mobile, and many times can be found on the outer surface of oxide scales—namely Ti and

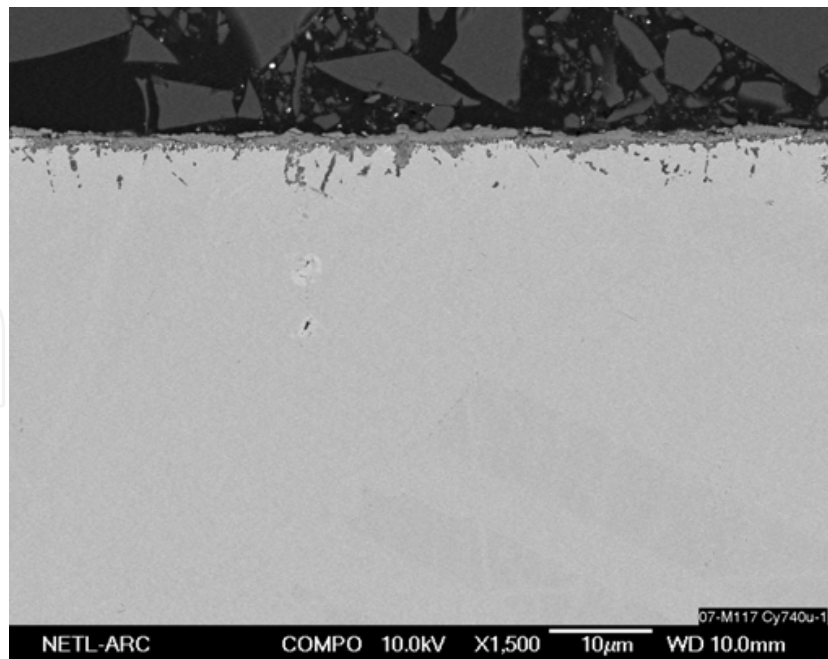


Fig. 9. Backscattered electron cross-section image after cyclic oxidation of Inconel 740 at 760 °C in air plus 37% H₂O after 2000 hourly cycles (Holcomb, 2009).

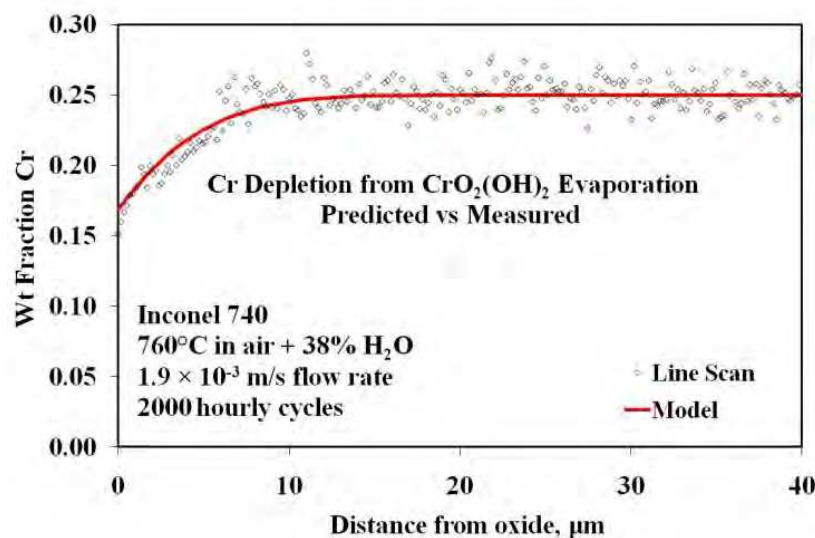


Fig. 10. Chromium depletion from cyclic oxidation of Inconel 740 at 760 °C in air plus 37% H₂O after 2000 hourly cycles. The individual points are from a line scan into the sample on the cross-section shown in Fig. 9 (Holcomb, 2009). The line results from the Eq. 12. The evaporation rate used in Eq. 12 was 8×10^{-10} kg/m²s, which corresponds to an $a_{\text{Cr}_2\text{O}_3}$ of 0.4.

Mn. For example, enough Mn additions to result in outer scales of Mn-Cr spinels instead of chromia is expected to reduce the evaporation of Cr by a factor of 55 at 700 °C and by a factor of 35 at 800 °C (Holcomb & Alman, 2006). This is equivalent to a chromia activity of 0.0006 at 760 °C. Prior work (Holcomb, 2009) showed that the higher evaporation rates shown by Haynes 230 and Inconel 740 corresponded to an $a_{\text{Cr}_2\text{O}_3}$ value of 0.05. The use of 0.05 in the analysis used for Fig. 10 results in a predicted evaporation rate of 2.8×10^{-10}

kg/m²s, and a wt fraction of Cr of 0.22 at the surface. Since some of the Cr loss can be attributed to the non-evaporated chromia scale, the best value for $a_{Cr_2O_3}$ lies between 0.05 and 0.4. Apparent $a_{Cr_2O_3}$ values, based on the negative slope of the mass change data, are shown in Table 3 for each alloy and condition in this study. Most of the apparent $a_{Cr_2O_3}$ values are within this range.

5. Hypothetical superheater-steam pipe-hp turbine steam path

The combination of gas evaporation of $CrO_2(OH)_2$, gas saturation of $CrO_2(OH)_2$, and Cr depletion in the alloy is illustrated in Fig. 11. Figure 11 represents one section of superheater (SH) tubing or steam pipe of cell length L. The bulk partial pressure of $CrO_2(OH)_2$ coming into the cell is $P_{CrO_2(OH)_2}^\circ$ (Incoming). Evaporation within the cell at rate k_e raises the $P_{CrO_2(OH)_2}^\circ$ (Outgoing) by the amount released by evaporation and is shown in Eq. 17.

$$P_{CrO_2(OH)_2}^\circ \text{ (Outgoing)} = P_{CrO_2(OH)_2}^\circ \text{ (Incoming)} + \frac{4k_e LRT}{duM_{CrO_2(OH)_2}} \tag{17}$$

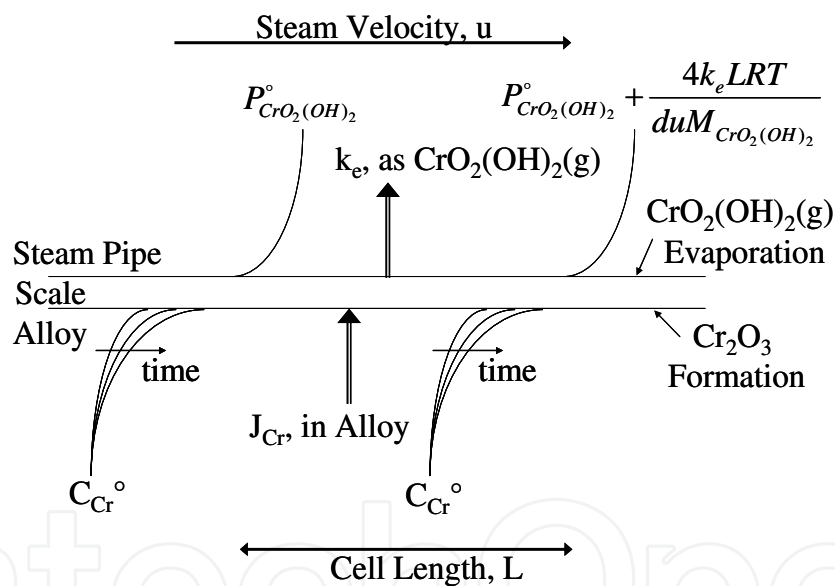


Fig. 11. The combination of gas evaporation of $CrO_2(OH)_2$, gas saturation of $CrO_2(OH)_2$, and Cr depletion in the alloy is illustrated. This represents one section of superheater tubing or steam pipe of cell length L (Holcomb, 2009).

The effects of saturating the gas phase with $CrO_2(OH)_2$ can then be calculated along the length of a SH tube or steam pipe by combining many cells together. A hypothetical arrangement of a 100 m long, 0.05 m I.D., SH that leads into a 50m long, 0.3 m I.D., steam pipe that leads to a high pressure (HP) turbine is illustrated in Fig. 12. The temperature profile and steam velocities are shown on the left-hand axis, while the evaporation rate is shown on the right-hand axis. The evaporation rate is based on an $a_{Cr_2O_3}$ of 0.05. The SH and steam pipe each consisted of 160 cells of the type shown in Fig. 11. Saturation results in an 80% reduction in the evaporation rate at the HP turbine. The steam chemistry used in Fig. 12 and in subsequent calculations was based off of feedwater

treatments that are typical of once-through supercritical power plants, i.e., a pH of 8.0-8.5 controlled with ammonia additions (Babcock & Wilcox, 1992). At high temperatures, water undergoes dissociation to O_2 and H_2 to levels well above 1 ppb. To estimate the dissolved oxygen required for Eq. 1 at temperature and pressure, the program FactSage 5.5 (Bale et al., 2007) was used to first determine the amount of NH_3 required for a pH of 8.25 at 25°C: 34.5 ppb. This agreed well with the reported (Babcock & Wilcox, 1992) 20-65 ppb NH_3 used for pH control to 8.0 to 8.5. Next FactSage 5.5 was used to find the value of the fugacities of H_2O and O_2 for each temperature and pressure combination from water with 34.5 ppb NH_3 . The use of fugacities instead of partial pressures made only a minor difference because the fugacity adjustments tended to cancel each other out.

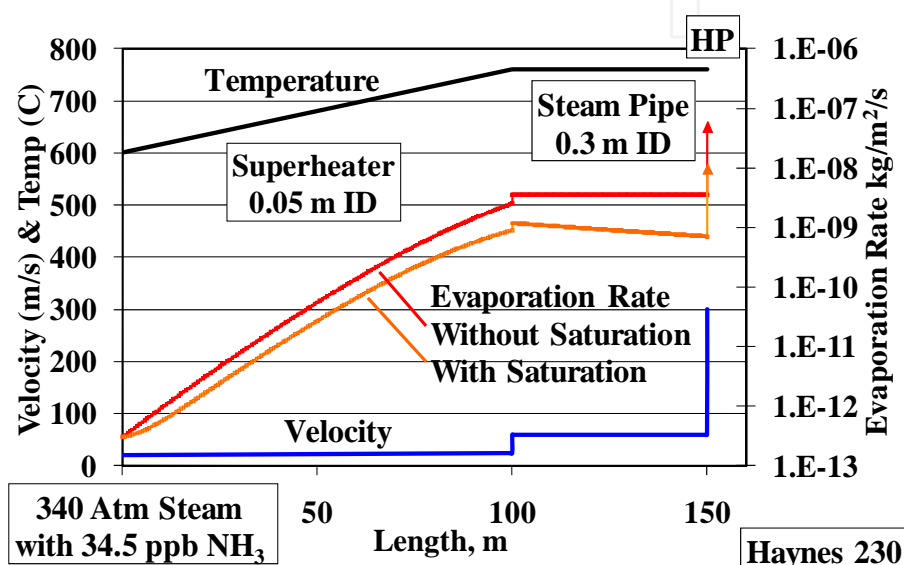


Fig. 12. The effects of gas saturation is shown for a hypothetical arrangement of a 100m long SH that leads into a 50m steam pipe that leads to a high pressure (HP) turbine. Saturation results in a 80% reduction in the evaporation rate at the HP turbine. An $a_{Cr_2O_3}$ of 0.05 was used. Adapted from Holcomb (2009).

The time for the alloy Cr level to reach zero at the scale-metal interface, using Eq. 14, is shown in Fig. 13 for the same conditions as in Fig. 12 (and using saturated values for k_e). Haynes 230 was the alloy used. Under this simulation the chromia evaporation at the HP turbine blade is expected to be so great as to deplete the alloy surface of Cr in a few days. However, the very high rates of evaporation predicted at the HP turbine will likely be less than the model. The model is highly dependent upon the chromia activity term, especially in combination with the saturation effect. Should the higher evaporation rate at the HP lead to a lower chromia activity (while keeping the $a_{Cr_2O_3}$ in the SH and steam pipe at 0.05), then the equilibrium surface $P_{Cr_2(OH)_2}$ can easily drop below $P_{Cr_2(OH)_2}^\circ$, and thus stop chromia evaporation (Eq. 9). In this example (with the $a_{Cr_2O_3}$ in the SH and steam pipe at 0.05), an $a_{Cr_2O_3}$ in the HP turbine section of 0.032 would be sufficiently low enough to stop chromia evaporation in the HP turbine.

The very high temperatures and total pressures of Figs. 12-13 match that of the U. S. Department of Energy's goals of 760 °C and 340 atm. The impact of evaporation at lower temperatures and pressures can be seen in Figs. 14-15, where similar procedures are used to estimate the time it takes for the surface concentration of Cr in the alloy to reach zero. In all

cases the SH inlet temperature was taken to be 600 °C. Below 600 °C, ferritic alloys, which would not be expected to form chromia scales, would typically be used.

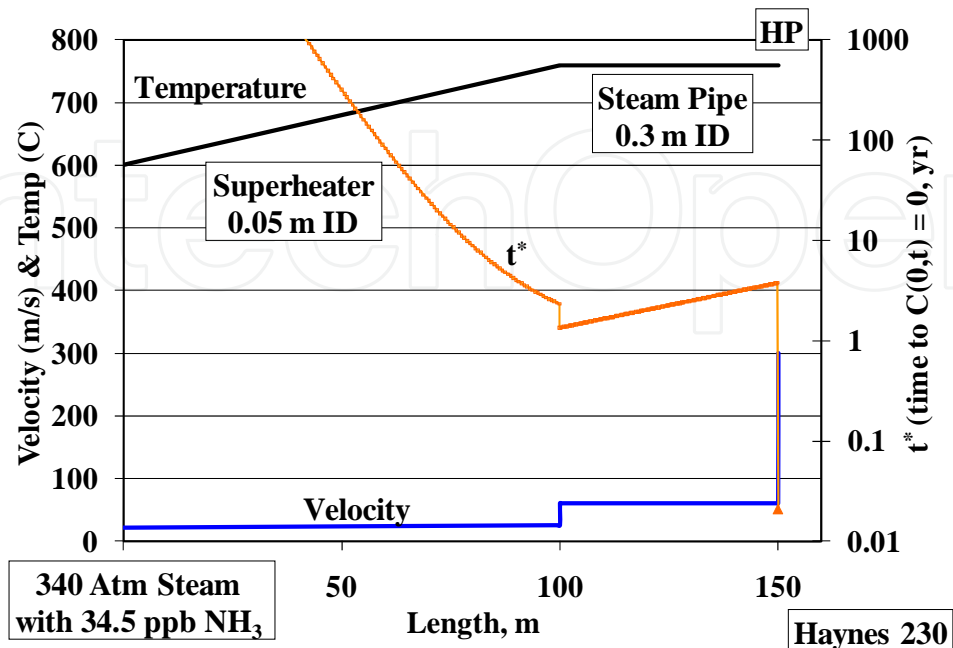


Fig. 13. The predicted time for the Cr level at the scale-metal interface to reach zero. Haynes 230 was the alloy system used in this estimate. An $a_{Cr_2O_3}$ of 0.05 was used. Adapted from Holcomb (2009).

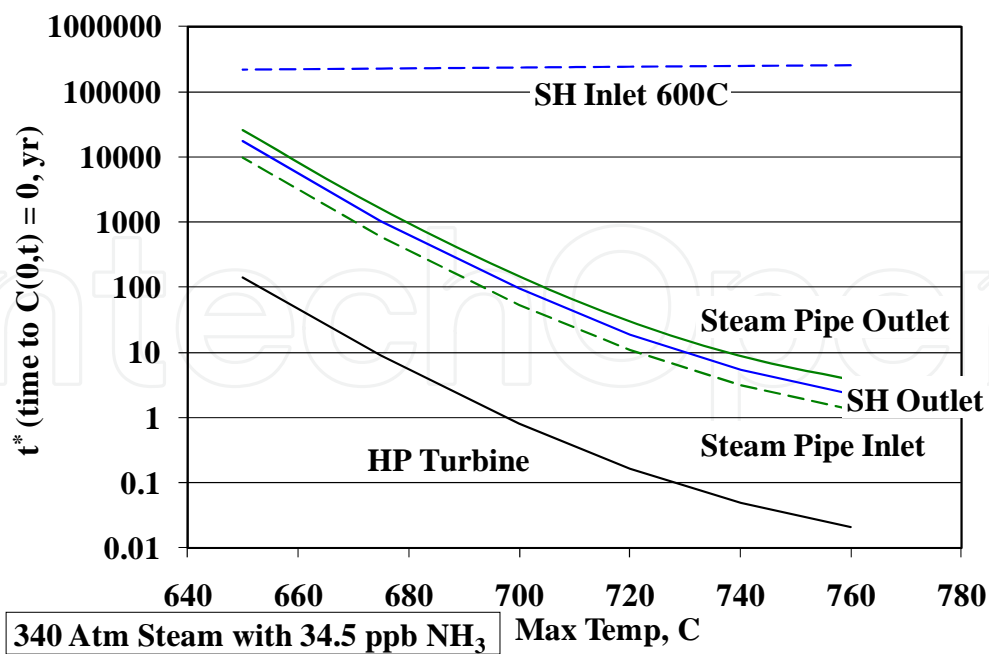


Fig. 14. The effects of temperature on the estimate of the time it takes for the surface concentration of Cr in the alloy to reach zero, at 340 atm. Haynes 230 was the alloy system used in this estimate. An $a_{Cr_2O_3}$ of 0.05 was used. Adapted from Holcomb (2009).

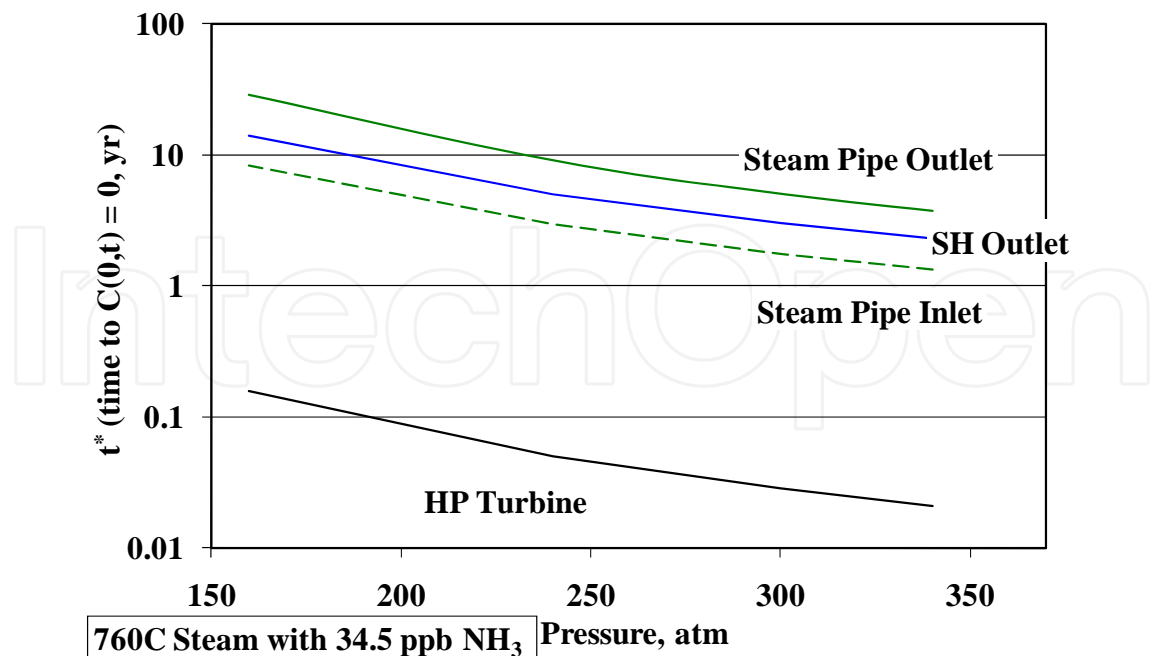


Fig. 15. The effects of pressure on the estimate of the time it takes for the surface concentration of Cr in the alloy to reach zero, at 760 °C. Haynes 230 was the alloy system used in this estimate. An $a_{\text{Cr}_2\text{O}_3}$ of 0.05 was used. Adapted from Holcomb (2009).

Figure 14 shows why chromia evaporation is not considered to be of much concern in existing steam boilers and turbines. Modern advanced steam cycles are currently no higher than 630 °C, so the time to breakaway oxidation (for which the time for $C(0,t)$ to reach 0 is being used as an estimate) is well beyond the life span of the boiler or turbine. Another factor limiting chromia evaporation in modern advance steam cycles is that ferritic steels are extensively used, and they do not form chromia scales. So the activity of Cr is lower in the scales, which from Eq. 1 lowers the partial pressure of $\text{CrO}_2(\text{OH})_2(\text{g})$, which in turn decreases chromia evaporation (Eq. 9).

6. Mitigation

As discussed in the Hypothetical Superheater-Steam Pipe-HP Turbine Steam Path section, relatively small changes in chromia activity at the oxide-steam interface can greatly influence the amount of chromia evaporation. For the alloys of interest, which contain Ti and/or Mn, large evaporation rates may be self-correcting as chromia is lost from the surface and concentrates Ti and Mn oxides (and thus reduces the chromia activity). Decreases in chromia activity along the steam path can result in little or no evaporation if the steam becomes saturated in $\text{Cr}_2(\text{OH})_2$ relative to the lower surface $\text{PCr}_2(\text{OH})_2$ that arises from the lower $a_{\text{Cr}_2\text{O}_3}$.

Another mitigation would be the use of a non-chromia forming coating. An example would be a thermal barrier coating (TBC), such as one based on yttria stabilized zirconia (YSZ). Such coatings are being postulated for use to reduce turbine blade erosion. This would eliminate the transport path for chromia evaporation. Even if the coating were porous, it would effectively increase the gaseous diffusion boundary layer to the thickness of the coating, thus eliminating much of the detrimental gas velocity effects.

7. Conclusions

A methodology was developed to calculate Cr evaporation rates from Cr_2O_3 with a flat planar geometry (Holcomb, 2008), was expanded upon to allow for interior cylindrical geometries, and to allow for the effects of $\text{CrO}_2(\text{OH})_2$ saturation within the gas phase (Holcomb, 2009). This approach was combined with Cr diffusion calculations within the alloy (with a constant flux of Cr leaving the alloy from evaporation) to predict Cr concentration profiles as a function of exposure time and to predict the time until the alloy surface concentration of Cr reaches zero.

An important aspect of chromia evaporation in alloys of interest (that contain Mn and Ti) is the possibility of reduced chromia activity at the metal surface. A reduction in chromia activity will reduce chromia evaporation. It was found that increasing the gas flow rate led to increased chromia evaporation and decreased apparent chromia activity. Increasing the water content in the moist air increased the evaporation, but results were mixed with its effect on chromia activity.

A hypothetical super heater (SH) tube, steam pipe, and high pressure (HP) turbine steam path was assembled and examined with the methodology. At the U. S. Department of Energy's goals of 760 °C and 340 atm, the time until breakaway oxidation was predicted to be quite short for the turbine blade, and of concern within the steam pipe and the higher temperature portions of the SH tube. The predicted time until breakaway oxidation increases dramatically with decreases in temperature and total pressure. However, it was shown that chromia activity variability within the steam path (i.e., chromia activity in the HP lower than that in the SH/steam pipe) could reduce or eliminate chromia evaporation. The steam could become saturated in $\text{Cr}_2(\text{OH})_2$ relative to the lower partial pressure of $\text{Cr}_2(\text{OH})_2$ at the metal surface (lowered by the lower chromia activity). Thus the higher expected chromia evaporation rates in the HP section could be self-mitigating as the loss of chromia from the scale, which increases the relative amounts of Ti and Mn oxides) reduces the chromia activity at the oxide surface.

8. References

- Asteman, H., Svensson, J.-E., Johansson, L.-G. & Norell, M. (1999). Indication of Chromium Oxide Hydroxide Evaporation during Oxidation of 304L at 873 K in the Presence of Water Vapor. *Oxidation of Metals*, Vol. 52, Nos. 1-2, (August 1999), pp. 95-111, ISSN 0030-770X.
- Asteman, H., Svensson, J.-E., Norell, M., & Johansson, L.-G. (2000). Influence of Water Vapor and Flow Rate on the High Temperature Oxidation of 304L; Effect of Chromium Oxide Hydroxide Evaporation. *Oxidation of Metals*, Vol. 54, Nos. 1-2, (August 2000), pp. 11-26, ISSN 0030-770X.
- Bale, C.W., Pelton, A.D., Thompson, W.T., Eriksson, G., Hack, K., Chartrand, P., Decterov, S., Melançon, J. & Petersen, S. (2007). FactSage 5.5, Thermfact and GTT-Technologies (2007).
- Bird, R.B., Stewart, W.E. & Lightfoot, E.D. (1960). *Transport Phenomena*, John Wiley & Sons, ISBN 0-471-41077-2, New York.
- Essuman, E., Meier, G.H., Żurek, J., Hänsel, M. & Quadackers, W. J. (2008). The Effect of Water Vapor on Selective Oxidation of Fe-Cr Alloys. *Oxidation of Metals*, Vol. 69, Nos. 3-4, (April, 2008), pp. 143-162, ISSN 0030-770X.

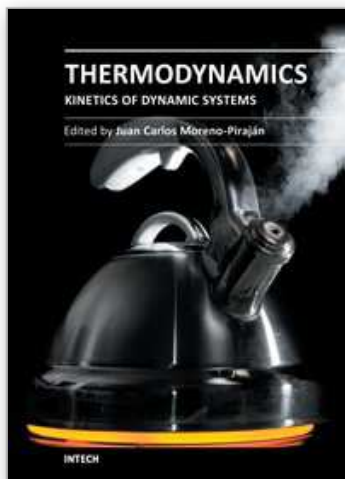
- Fuller, E.N., Schettler, P.D. & Giddings J.C. (1966). *Industrial & Engineering Chemistry*, Vol. 58, No. 5, (May, 1966), pp. 19-27, ISSN 1226-086X.
- Gaskell, D.R. (1992). *An Introduction to Transport Phenomena in Materials Engineering*, Macmillan Publishing, ISBN 0-02-340720-4, New York.
- Gindorf, C., Hilpert, K., & L. Singheiser, L. (2001). Determination of Chromium Vaporization Rates of Different Interconnect Alloys by Transpiration Experiments, In: *Solid Oxide Fuel Cells (SOFC VII)*, Yokokawa, H. & Singhal, S.C. (Eds.), PV 2001-16, pp. 793-802, The Electrochemical Society Proceedings Series, ISBN 978-1-56677-322-5 Pennington, NJ.
- Graham, H.C. & Davis, H.H. (1971). Oxidation/Vaporization Kinetics of Cr₂O₃. *Journal of the American Ceramic Society*, Vol. 54, No. 2, (February 1971), pp. 89-93. ISSN 0002-7820.
- Haynes International. (2008a). Haynes 230 Alloy, H-3135C, Haynes International, Kokomo, IN.
- Haynes International. (2008b). Haynes 282 Alloy, H-3172A, Haynes International, Kokomo, IN.
- Holcomb, G.R. (2008). Calculation of Reactive-Evaporation Rates of Chromia. *Oxidation of Metals*, Vol. 69, Nos. 3-4, (April 2008), pp. 163-180, ISSN 0030-770X.
- Holcomb, G.R. (2009). Steam Oxidation and Chromia Evaporation in Ultrasupercritical Steam Boilers and Turbines. *Journal of the Electrochemical Society*, Vol. 156, No. 9, (September, 2009), pp. C292-C297. ISSN 0013-4651.
- Holcomb, G.R. & Alman, D.E. (2006). Effect of Manganese Additions on the Reactive Evaporation of Chromium in Ni-Cr Alloys, *Scripta Materialia*, Vol. 54, No. 10, (May, 2006), pp. 1821-1825, ISSN 1059-9495.
- Holcomb, G.R., Alman, D.E., Doğan, Ö.N., Rawers, J.C., Schrems, K.K. & Ziomek-Moroz, M. (2007). Steam Turbine Materials and Corrosion. *Proceedings of the 21st Annual Conference on Fossil Energy Materials*, Knoxville, TN, April 30-May 1, 2007.
- Incropera, F.P. & DeWitt, D.P. (2001). *Fundamentals of Heat and Mass Transfer* (5th edition), John Wiley & Sons, ISBN 978-0471386506, New York.
- Kubaschewski, O. & Alcock, C.B. (1979). *Metallurgical Thermochemistry* (5th edition), Pergamon Press, ISBN 0080221076, New York.
- Masuyama, F. (2001). History of Power Plants and Progress in Heat Resistant Steels, *ISIJ International*, Vol. 41, (June, 2001), No. 6, pp. 612-625, ISSN 0915-1559.
- Meier, G.H., Jung, K., Mu, N., Yanar, N.M., Pettit, F.S., Abellán, J.P., Olszewski, T., Quadackers, W.J. & Holcomb, G.R. (2010). Effect of Alloy Composition and Exposure Conditions on the Selective Oxidation Behavior of Ferritic Fe-Cr and Fe-Cr-X Alloys. *Oxidation of Metals*, Vol. 74, Nos. 5-6, (November-December, 2010), pp. 319-340, ISSN 0030-770X.
- Opila, E.J., Myers, D.L., Jacobson, N.S., Nielsen, I.M.B., Johnson, D.F., Olminky, J.K. & Allendorf, M. D. (2007). Theoretical and Experimental Investigation of the Thermochemistry of CrO₂(OH)₂(g). *Journal of Physical Chemistry A*, Vol. 111, No. 10, (October 2007), pp. 1971-1980, ISSN 1089-5639.
- Paul, A.R., Kaimal, K.N.G., Naik, M.C. & Dharwadkar, S.R. (1994). Lattice and Grain Boundary Diffusion of Chromium in Superalloy Incoloy-800. *Journal of Nuclear Materials*, Vol. 217, (November, 1994), Nos. 1-2 pp. 75-81, ISSN 0022-3115.

- Peng, X., Yan, J., Zhou, Y. & Wang, F. (2005). Effect of Grain Refinement on the Resistance of 304 Stainless Steel to Breakaway Oxidation in Wet Air. *Acta Materialia*, Vol. 53, No. 19, (November, 2005), pp. 5079-5088, ISSN 1359-6454.
- Pettit, F.S. & Meier, G.H. (2006). Fundamental Studies of the Durability of Materials for Interconnects in Solid Oxide Fuel Cells, Final Report, DOE Award: DE FC26 02NT41578.
- Petukhov, B.S. (1970). Heat Transfer and Friction in Turbulent Pipe Flow with Variable Physical Properties, In: *Advances in Heat Transfer*, Vol 6, Irvine, T.F. & Hartnett, J.P. (Eds.), p. 503-564, Academic Press, ISBN 978-0120200061, New York.
- Royal Institute of Technology, Foundation of Computational Thermodynamics. (1999). MOB2, Mobility Database, Version 2.0, Royal Institute of Technology, Foundation of Computational Thermodynamics, Stockholm, Sweden.
- Saunders, N. (2000). Ni-DATA, Version 7, Thermotech Ltd, Surrey, UK.
- Slattery, J.C. & Bird, R.B. (1958). *American Institute of Chemical Engineers Journal*, Vol. 4, No. 2, (june, 1958), pp. 137-142, ISSN 0001-1541.
- Special Metals Corporation. (2004a). Inconel Alloy 740, SMC-090, Special Metals Corporation, Huntington, WV.
- Special Metals Corporation. (2004b). Nimonic Alloy 263, SMC-054, Special Metals Corporation, Huntington, WV.
- Special Metals Corporation. (2005). Inconel Alloy 617, SMC-029, Special Metals Corporation, Huntington, WV.
- Special Metals Corporation. (2006). Inconel Alloy 625, SMC-063, Special Metals Corporation, Huntington, WV.
- Stultz, S.C. & Kitto, J.B. (Eds.) (1992). *Steam* (40th edition), Babcock & Wilcox, ISBN 0963457004, Barberton, Ohio.
- Tedman, C.S., Jr. (1966). The Effect of Oxide Volatilization on the Oxidation Kinetics of Cr and Fe-Cr Alloys. *Journal of the Electrochemical Society*, Vol. 113, No. 8, (August 1966), pp. 766-768, ISSN 0013-4651.
- Thermo-Calc Software AB. (2006). DICTRA, Diffusion Simulation Software, Version 24, Thermo-Calc Software AB, Stockholm, Sweden.
- Viswanathan, R., Henry, J.F., Tanzosh, J., Stanko, G., Shingledecker, J., Vitalis, B & Purgert, R. (2005). U.S. Program on Materials Technology for Ultra-Supercritical Coal power Plants. *Journal of Materials Engineering and Performance*, Vol. 14, No. 3, (June 2005), pp. 281-292, ISSN 1059-9495.
- Whittle, D.P., Evans, D.J., Scully, D.B. & Wood, G.C. (1967a). Compositional Changes in the Underlying Alloy during the Protective Oxidation of Alloys. *Acta Metallurgica*. Vol. 15, No. 9, (September, 1967), pp. 1421-1430, ISSN 1359-6454.
- Whittle, D.P., Wood, G.C., Evans, D.J. & Scully, D.B. (1967b). Concentration Profiles in the Underlying Alloy during the Oxidation of Iron-Chromium Alloys. *Acta Metallurgica*, Vol. 15, No. 11, (November, 1967), pp. 1747-1755, ISSN 1359-6454.
- Winterton, R.H.S. (1998). Where did the Dittus and Boelter Equation Come From? *International Journal of Heat and Mass Transfer*, Vol. 41, Nos. 4-5, (February-March, 1998), pp. 809-810, ISSN 0017-9310.
- Wright, A.I.G. & Tortorelli, P.F. (2007). Program on Technology Innovation: Oxide Growth and Exfoliation on Alloys Exposed to Steam, Report 1013666, EPRI, Palo Alto, CA.

Young, D.J. & Pint, B.A. (2006). Chromium Volatilization Rates from Cr₂O₃ Scales into Flowing Gases Containing Water Vapor. *Oxidation of Metals*, Vol. 66, Nos. 3-4, (October, 2006), pp. 137-153, ISSN 0030-770X.

IntechOpen

IntechOpen



Thermodynamics - Kinetics of Dynamic Systems

Edited by Dr. Juan Carlos Moreno Piraján

ISBN 978-953-307-627-0

Hard cover, 402 pages

Publisher InTech

Published online 22, September, 2011

Published in print edition September, 2011

Thermodynamics is one of the most exciting branches of physical chemistry which has greatly contributed to the modern science. Being concentrated on a wide range of applications of thermodynamics, this book gathers a series of contributions by the finest scientists in the world, gathered in an orderly manner. It can be used in post-graduate courses for students and as a reference book, as it is written in a language pleasing to the reader. It can also serve as a reference material for researchers to whom the thermodynamics is one of the area of interest.

How to reference

In order to correctly reference this scholarly work, feel free to copy and paste the following:

Gordon R. Holcomb (2011). Chromia Evaporation in Advanced Ultra-Supercritical Steam Boilers and Turbines, Thermodynamics - Kinetics of Dynamic Systems, Dr. Juan Carlos Moreno Piraján (Ed.), ISBN: 978-953-307-627-0, InTech, Available from: <http://www.intechopen.com/books/thermodynamics-kinetics-of-dynamic-systems/chromia-evaporation-in-advanced-ultra-supercritical-steam-boilers-and-turbines>

INTECH

open science | open minds

InTech Europe

University Campus STeP Ri
Slavka Krautzeka 83/A
51000 Rijeka, Croatia
Phone: +385 (51) 770 447
Fax: +385 (51) 686 166
www.intechopen.com

InTech China

Unit 405, Office Block, Hotel Equatorial Shanghai
No.65, Yan An Road (West), Shanghai, 200040, China
中国上海市延安西路65号上海国际贵都大饭店办公楼405单元
Phone: +86-21-62489820
Fax: +86-21-62489821

© 2011 The Author(s). Licensee IntechOpen. This chapter is distributed under the terms of the [Creative Commons Attribution-NonCommercial-ShareAlike-3.0 License](#), which permits use, distribution and reproduction for non-commercial purposes, provided the original is properly cited and derivative works building on this content are distributed under the same license.

IntechOpen

IntechOpen